



PAPER

Subtractive fabrication of ferroelectric thin films with precisely controlled thickness

To cite this article: Anton V levlev *et al* 2018 *Nanotechnology* **29** 155302

View the [article online](#) for updates and enhancements.

You may also like

- [Recent progress in bio-inspired macrostructure array materials with special wettability—from surface engineering to functional applications](#)
Zhongxu Lian, Jianhui Zhou, Wanfei Ren et al.
- [Subtractive transfer printing process for rapid fabrication of Au nano/micro structures on a polymer substrate](#)
Hao Shen, Yuki Nakagawa and Masahiko Yoshino
- [Leading edge topography of blades—a critical review](#)
Robert J K Wood and Ping Lu





ECS The Electrochemical Society
Advancing solid state & electrochemical science & technology

247th ECS Meeting
Montréal, Canada
May 18-22, 2025
Palais des Congrès de Montréal

Showcase your science!

Abstracts due December 6th

Subtractive fabrication of ferroelectric thin films with precisely controlled thickness

Anton V Ievlev^{1,2} , Marius Chyasnavichyus^{1,2}, Donovan N Leonard³, Joshua C Agar⁴, Gabriel A Velarde⁴, Lane W Martin^{4,5}, Sergei V Kalinin^{1,2} , Petro Maksymovych^{1,2} and Olga S Ovchinnikova^{1,2}

¹ The Center for Nanophase Materials Sciences, Oak Ridge National Laboratory, 1 Bethel Valley Rd., Oak Ridge, TN 37831, United States of America

² Institute for Functional Imaging of Materials, Oak Ridge National Laboratory, 1 Bethel Valley Rd., Oak Ridge, TN 37831, United States of America

³ Materials Science and Technology Division, Oak Ridge National Laboratory, 1 Bethel Valley Rd., Oak Ridge, TN 37831, United States of America

⁴ Department of Materials Science and Engineering, University of California Berkeley, Berkeley, CA 94720, United States of America

⁵ Materials Sciences Division, Lawrence Berkeley National Laboratory, Berkeley, CA 94720, United States of America

E-mail: ievlevav@ornl.gov

Received 12 December 2017, revised 15 January 2018

Accepted for publication 2 February 2018

Published 22 February 2018



Abstract

The ability to control thin-film growth has led to advances in our understanding of fundamental physics as well as to the emergence of novel technologies. However, common thin-film growth techniques introduce a number of limitations related to the concentration of defects on film interfaces and surfaces that limit the scope of systems that can be produced and studied experimentally. Here, we developed an ion-beam based subtractive fabrication process that enables creation and modification of thin films with pre-defined thicknesses. To accomplish this we transformed a multimodal imaging platform that combines time-of-flight secondary ion mass spectrometry with atomic force microscopy to a unique fabrication tool that allows for precise sputtering of the nanometer-thin layers of material. To demonstrate fabrication of thin-films with *in situ* feedback and control on film thickness and functionality we systematically studied thickness dependence of ferroelectric switching of lead-zirconate-titanate, within a single epitaxial film. Our results demonstrate that through a subtractive film fabrication process we can control the piezoelectric response as a function of film thickness as well as improve on the overall piezoelectric response versus an untreated film.

Keywords: ferroelectrics, thin films, ion beam fabrication, time-of-flight secondary ion mass spectrometry, atomic force microscopy

(Some figures may appear in colour only in the online journal)

Introduction

The ability to control thin-film growth has led to advances in our understanding of fundamental physics as well as to the emergence of novel technologies including giant magnetoresistance materials and devices [1–5], ferroelectric tunneling barriers and capacitors [6–9], superconductor oxides of Josephson junctions [10, 11], quantum computing [12–14],

and more exotic systems. The rapid improvement of modern electronics hinges on the development of novel methodologies to process materials at ever shrinking dimensions. Processing techniques that allow for monolayer precision control during the growth process like pulsed-laser deposition [15] and atomic-layer deposition [16] grow materials in accordance with fundamental physics and often provide only certain terminations at the film interface and surface.

Additionally, when using these approaches dislocations and vacancies will migrate to the interface of the films when high enough temperatures are reached causing problems for controlling the chemistry of the interface as well as leading to surface instabilities and contamination [17]. Altogether, these factors may hamper fundamental investigations and practical applications of thin film systems we can produce.

Here we open a new direction for research in complex oxides by demonstrating a subtractive fabrication process that enables creation and modification of thin films with pre-defined thicknesses. It allows us to elucidate the properties of oxides while simultaneously minimizing the effects of contaminants. We apply a combination of time-of-flight secondary ion mass spectrometry (ToF-SIMS) [18–21] with atomic force microscopy (AFM) for precise sputtering of the nanometer-thin layers of material. The sputtering process is realized by the ion beam under control of mass spectrometry. AFM is further utilized for sputtering depth calibration. To verify this technique, we systematically investigated thickness dependence of ferroelectric switching of lead-zirconate-titanate, with just one epitaxial film as a source of materials. Surprisingly, we observe not only robust switching in pre-sputtered films, but also strong improvement of piezoelectric response once the aged surface layer is removed.

Experiment and results

As a model system, we used a 100 nm thick ferroelectric film of lead zirconate titanate $\text{PbZr}_{0.2}\text{Ti}_{0.8}\text{O}_3$ (PZT) grown on a SrTiO_3 (STO) (001) substrate with a 50 nm thick SrRuO_3 (SRO) buffer layer. ToF-SIMS was used to clean the PZT surface and adjust its thickness. Measurements have been performed using a TOF.SIMS.5 NSC (ION-TOF GmbH) instrument, combining ToF-SIMS and AFM in the same vacuum chamber. Mass spectrometry measurements have been done by a focused O_2^- sputtering source (500 eV energy, 100 nA current, and $\sim 20 \mu\text{m}$ spot size) and a Bi^+ primary gun (30 keV energy, 30 nA current, and $\sim 5 \mu\text{m}$ spot size). Sputtered regions were further analyzed in a built-in AFM chamber to measure the absolute values of the sputtering depth. External AFM (Icon Bruker) and STEM (Titan, FEI) were also used to compare crystallography and ferroelectric properties of pristine and treated regions.

As a first step, we performed depth profiling of the PZT locally, which revealed the total film thickness, and the local chemical composition of surface layer and the film. We used O_2^- sputtering over $300 \times 300 \mu\text{m}$ regions with cycle of 10 s. Each cycle was accompanied by ToF-SIMS surface chemistry analysis using the focused Bi^+ primary ion source and the time-of-flight analyzer in positive ion-detection mode. The mass spectra are therefore collected from each layer, enabling depth profiling of the chemical composition.

The averaged mass spectrum of the PZT film and part of SRO buffer (figure 1) clearly shows peaks of the PZT base elements (Pb^+ , Zr^+ and Ti^+), their oxides (PbO^+ , ZrO^+ and TiO^+), Sr^+ and Ru^+ from the SRO buffer layer as well as elements from an adsorption surface layer (Na^+ , K^+ , etc). The

area of those peaks has been used to plot depth profiles of their bulk distribution (figure 2(a)). One should note that the x -axis in figure 1 is not the physical depth, but the sputter time, which is directly proportional to the sputter depth (the longer sputtering time the deeper the crater). These profiles show sharp transition from PZT to SRO (decrease of Pb^+ , Zr^+ , Ti^+ and increase of Sr^+ signals) at around 840 s of sputtering. This can be used to roughly estimate the sputtering rate of PZT: $v_{\text{PZT}} \sim 0.12 \pm 0.01 \text{ nm s}^{-1}$.

We further performed precise calibration of the sputtering depth using the AFM built-in to the ToF-SIMS vacuum chamber. The AFM measurements were performed in contact mode inside the regions sputtered for different times from 210 to 930 s. The crater topography profiles were used for sputtering depth calibration (figure 2(b)). These measurements were carried out in automated profiling mode. In this mode resulted crater profile (300 μm long) is measured by sections of 80 μm . Sections are measured with overlap of 15% and further automatically stitched. Experiments demonstrated that the sputtering is linear with time within the film, and the value of the sputtering rate based on the AFM data is identical to that estimated from the ToF-SIMS depth profiles. In addition, we used macroscopic data of the film thickness and measured profile for the longest sputter to estimate the sputtering rate of the SRO buffer layer. The obtained value $v_{\text{SRO}} \sim 0.028 \text{ nm s}^{-1}$ was found to be significantly lower than the sputtering rate of PZT. Hereinafter we will reference sputtering depth in percentage from initial film thickness, based on the sputtering time and the macroscopic data of the film thickness (figure 2(a)). Analysis of the depth profiles also showed slight increase in the roughness of sputtered region (figure 2(d)). Root mean squared R_q value of the roughness is used. However, total roughness change does not exceed 1.5 nm, which cannot significantly affect properties of the modified sample.

The results of this work reveal that the sputtering process by ToF-SIMS under the control of mass spectrometry can act as a subtractive fabrication approach for the creation of thin films of pre-defined thickness and surface conditioning. We should note, that works on the ion beam thinning of ferroelectric thin films and single crystals were performed in the past, however those approaches led to damage of the crystallographic structure and degradation of ferroelectric properties [22–24]. To ascertain structural damages during this process and establish potential ionic damage we performed STEM and AFM measurements.

STEM was used to investigate the atomic structure of cross-sections of pristine and sputtered PZT samples (figure 3). In all cases these measurements clearly differentiate the surface layer, the PZT film, and the SRO/STO substrate. The pristine, as-grown sample, as expected, showed the presence of a thick ($\sim 10 \text{ nm}$) inhomogeneous aged surface layer (figure 3(a)). This layer is known to hamper local probing of ferroelectric properties by AFM and can lead to a number of non-trivial phenomena during polarization reversal [25–29]. Presence of this layer is confirmed by ToF-SIMS, which showed high concentration Na^+ , K^+ on the sample surface (figure 2(a)). The sputtering process removed this

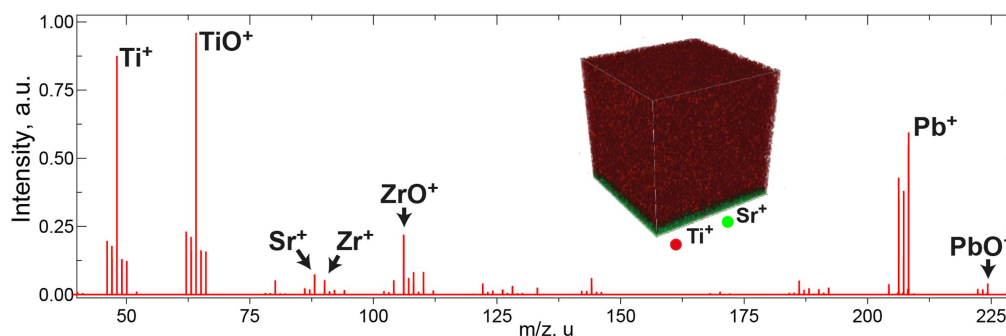


Figure 1. Averaged mass spectrum of studied films, averaged over whole thickness of PZT and part of SRO buffer layer. (inset) 3D overlay of Ti^+ (red) and Sr^+ (green) spatial distribution.

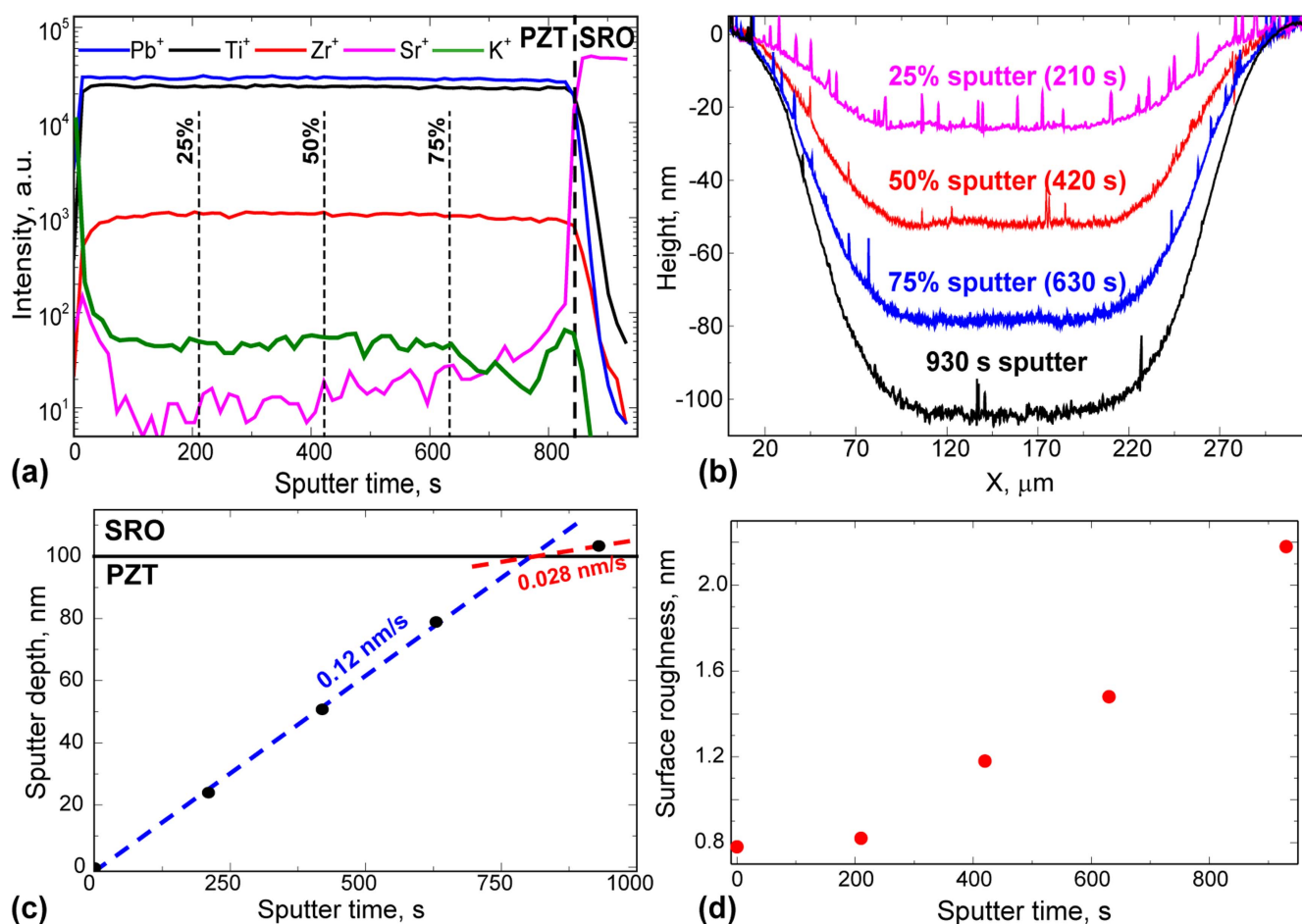


Figure 2. Depth profiling of PZT thin film. (a) ToF-SIMS depth profiles; (b) AFM topographical profiles of sputtered craters; (c) depth calibration; (d) roughness of the sputtered regions.

contamination layer (figures 3(b), (c)) and demonstrated consistency with designated sputtering times—the film thickness was ~ 52 nm after sputtering for 50% (figure 3(b)), and ~ 15 nm for 80% (figure 3(c)). Detailed STEM imaging showed that sputtering process does not change crystallography in the bulk of PZT and on the PZT/SRO interface (figure 3(d)), however it showed formation of the thin (~ 3 nm) amorphous layer (figure 3(e)). At this point, we cannot speculate about the origin of this amorphous layer, it could be formed during the sputtering process or just be an artifact of the cross-section preparation for STEM imaging.

We should note here, that thickness of this artificial layer is much smaller, than in the case of pristine PZT sample, so one would expect enhancement in the properties of modified films.

We further used the AFM to study ferroelectric and conductive properties of the treated regions and piezo-response force microscopy was used to study switching. The measurements were carried out over a grid of 10×10 points with an area of $5 \times 5 \mu\text{m}$.

We used local hysteresis loops to characterize the ferroelectric properties of the sputtered PZT regions (figure 4).

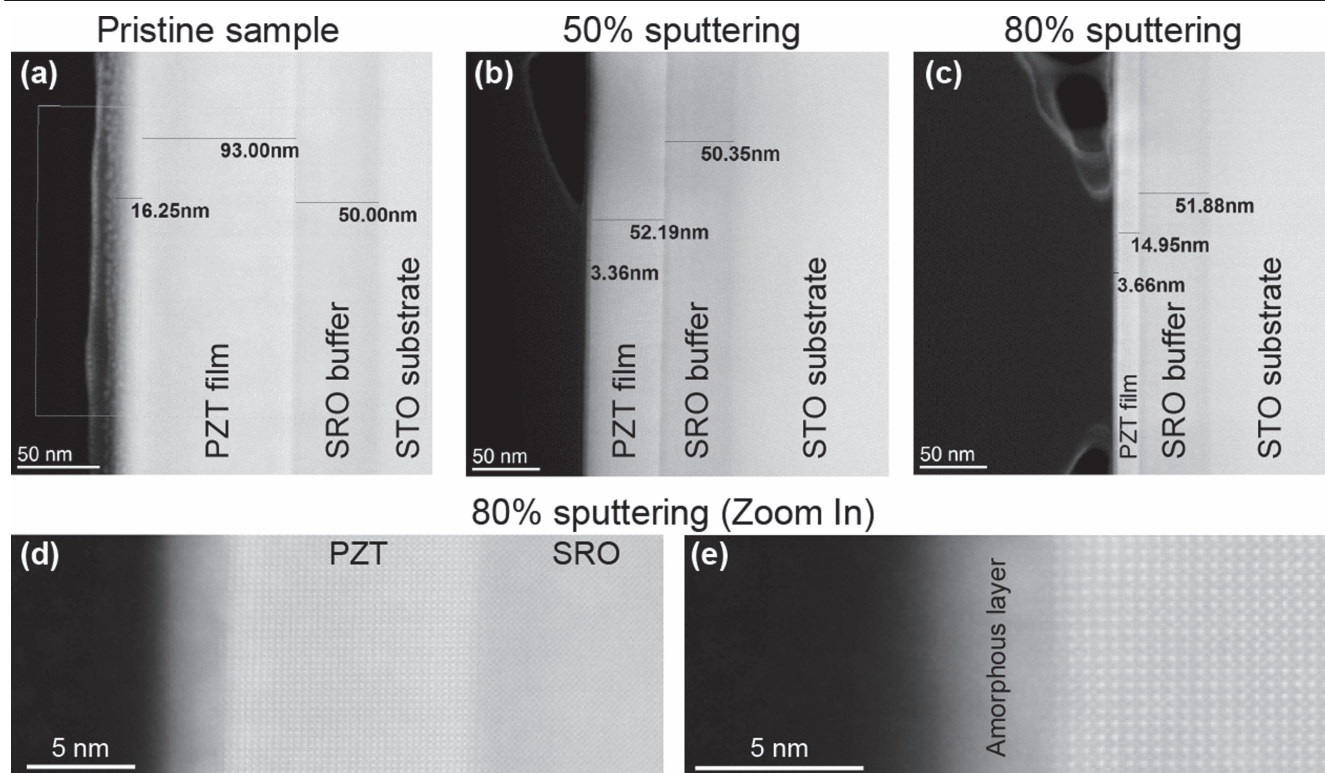


Figure 3. STEM imaging of the cross-sections of the pristine (a) and sputtered (b)–(e) PZT thin film. Sputtering depth corresponds to 50% (b) and 80% (c)–(e) of the film thickness.

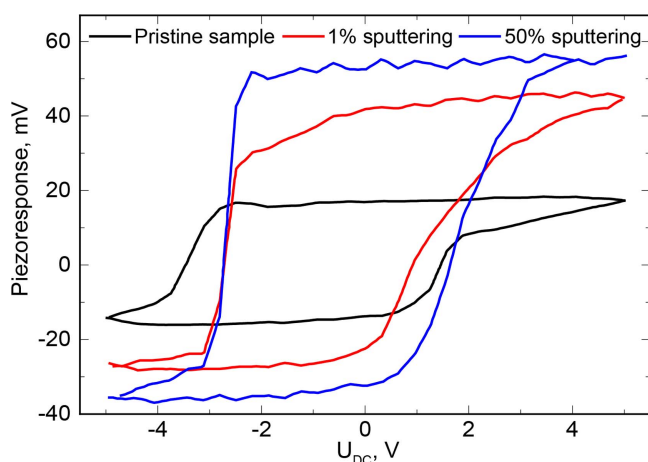


Figure 4. Local hysteresis loops measured in pristine sample and regions sputtered for 1% and 50% of the film thickness.

These loops are measured during application of the DC voltage to the tip and are able to characterize ferroelectric switching in the nanometer region underneath the tip under the action of external DC field produced by the tip. Details about measurements of the local hysteresis loops and their interpretation can be found in [30–35].

Careful analysis of the averaged loops measured at the sputtered regions clearly showed hysteresis, which confirms that the film remains ferroelectric, as polarization can be switched by application of an external electric field. Furthermore, the coercive voltage (loop width on the half max) was not significantly altered, ranging from 4 to 5 V for all

regions. Coercive voltage corresponds to the electric field required to reverse polarization underneath the tip and is one of the most important ferroelectric parameters.

At the same time, we found, that the total piezoresponse (full height of the loop), has been significantly affected. It *increased* more than twice from 31 mV for the pristine, as-grown sample to 71 ± 8 mV after a short sputtering process (1% of the film thickness) and to 90 ± 10 mV after sputtering of half the film thickness. We should note here that in this manuscript we measure piezoresponse in volts (mV), which is a deflection voltage reading from the AFM detector, which is directly proportional to deflection of the tip and piezoelectric deformation of the surface.

Increase in the total piezoresponse is in a good agreement with the STEM results, showing the presence of a significant adsorption layer on the surface of the pristine, as-grown sample (figure 3(a)). In this case, piezoresponse of the pristine sample is reduced due to the presence of the adsorption layer. This leads to decrease in the sensitivity of PFM measurements and correspondingly decreases piezoresponse. At the same time, ferroelectric properties of the film stay unchanged, which is confirmed by the loop shape and values of coercive field.

To characterize the conductive properties of the modified regions we performed current measurements through the AFM tip (figure 5). These measurements did not show any significant changes in the film electro-conductivity up to 90% of the sputtering (figure 5(a)). The corresponding resistivity was around 1–10 G Ω . However, further decreasing the residual film thickness down to 10% of the initial thickness led to

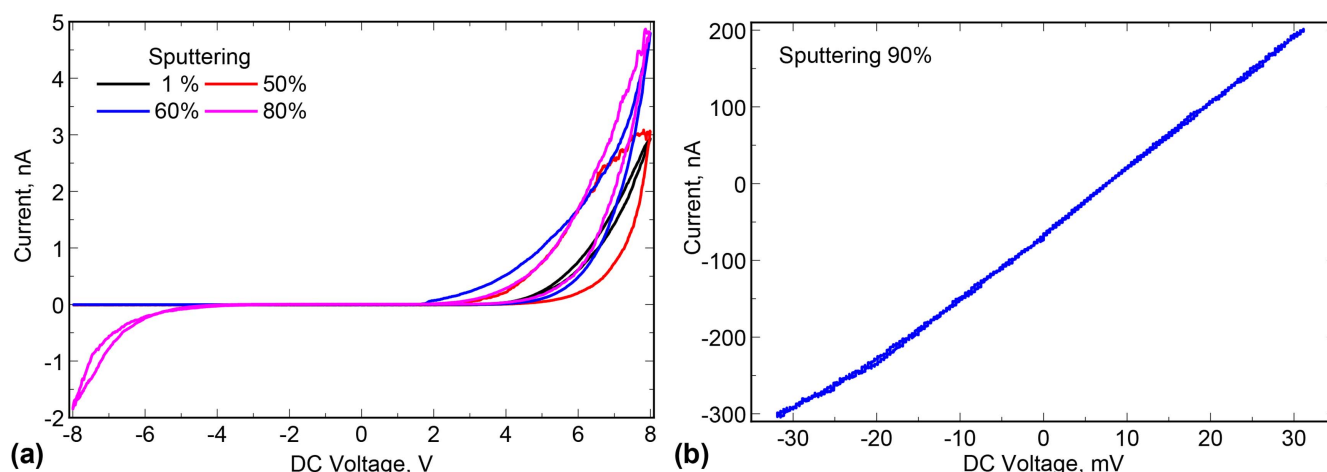


Figure 5. Local current measurements by biased AFM tip in sputtered regions of PZT thin film. (a) Sputtering of 1%–80% and (b) 90% of the film thickness.

abrupt increase of the current (to 100 nA) with corresponding resistivity $\sim 1 \text{ M}\Omega$ (figure 5(b)). This phenomenon is related with the proximity of the conductive SRO buffer layer and demonstrates the challenge of obtaining extremely thin (few unit-cell) films with the sputtering approach.

Methods

Time-of-flight secondary ion mass spectrometry

ToF-SIMS measurements have been done using TOF.SIMS.5-NSC instrument, using bismuth ion gun as a primary ion source and O_2^- ion gun as a sputter source.

Sputter was realized by O_2^- ion beam with energy of ions 1 keV, current 120 nA and spot size $\sim 20 \mu\text{m}$. To control sputtering process we analyzed mass spectra of the freshly sputtered surface in positive SIMS mode. In this case Bi liquid metal ion gun with energy of ions 30 keV, current $\sim 30 \text{ nA}$ and spot size $\sim 5 \mu\text{m}$. This allowed us to acquire mass spectra with spectral resolution below 0.01 Da.

Atomic force microscopy

Characterization of the depth and profiles of sputtered craters has been done using atomic force microscope Nanoscan introduced into the vacuum chamber of ToF-SIMS. Measurements were performed in contact AFM mode using Nanosensor PPP-EFM tips with force constant of 2.8 N m^{-1} and radius of curvature better than 25 nm.

Piezoresponse Force Microscopy and conductive AFM measurements were carried out in environmental conditions using Bruker Icon AFM and Budget Sensors 75E-G tips with force constant of 3 N m^{-1} and radius of curvature below 25 nm. In PFM measurements AC voltage with amplitude of 0.5 V and frequency about 300 kHz was applied to the tip in addition to switching DC voltage -5 to $+5 \text{ V}$. For local current measurements DC voltage was applied to the tip, while current has been measured using external current amplifier connected to the bottom electrode of the sample.

Scanning transmission electron microscopy

A Hitachi NB5000 FIB/SEM was used to prepare electron transparent foils of the PZT/SrTiO₃ thin film sample for STEM imaging. To protect the PZT surface from ion beam damage during preparation, the sample was coated with $\sim 200 \text{ nm}$ of carbon. Thinning to electron transparency begun with deposition of a $25 \mu\text{m}$ long, $4 \mu\text{m}$ wide, $\sim 500 \text{ nm}$ thick tungsten capping layer to reduce ‘curtaining’ during the final FIB thinning of the specimen. A 40 kV focused beam of Ga ions, with a current of 19.5 nA, was used to mill material away down into the substrate to a depth of $4\text{--}5 \mu\text{m}$. The sample was lifted from the bulk and transferred to a Cu Omniprobe half grid. A series of milling steps was then used to reduce the thickness of the lamella until it was electron transparent ($<100 \text{ nm}$). The thinning was started with a 40 kV, 3.36 nA beam and thinned the sample to $1 \mu\text{m}$ thick. For the final milling step the beam parameters were changed to 20 kV, 0.11 nA and the sample was thinned to $<100 \text{ nm}$ thick. To minimize Ga implantation effects and amorphous material on the surface of the FIB thinned sample, a Fischione Nanomill was operated at 900 eV with a 130 pA Ar^+ beam for ion milling of the sample at $\pm 10^\circ$ for 15 min each side.

High angle annular dark field (HAADF) imaging of the PZT films was performed at 100 kV with an aberration corrected scanning transmission electron microscope, the Nion UltraSTEM 100. For HAADF imaging an illumination half angle of $\sim 85 \text{ mrad}$ was used.

Conclusion

In conclusion, in this paper we developed a universal technique for subtractive fabrication of thin films with precisely controlled thickness. In this approach, a focused oxygen-ion beam is used for sputtering under the control of ToF-SIMS, which allows tuning of functional material response through for *in situ* surface cleaning and feedback on precise film thickness. This approach can be useful for fundamental investigations as well as practical application of various thin

films. In particular, it enables size-effects on collective phenomena and correlated atomic and electron states to be investigated within a single film, modified in certain regions by the ion beam. Our benchmark study of ferroelectric size effect in lead zirconate-titanate revealed the presence of a significant adsorption layer on the surface of pristine, as-grown samples leading to a decrease of the piezoelectric response, measured with an AFM tip. Oxygen sputtering completely removed this layer, enhancing piezoresponse 2–3 times compared to the as-grown state, while ferroelectric properties and crystallography of the film remained unchanged down to about 10% of the original thickness. These results point toward applicability of the developed approach for wider range of thin-films and practical applications.

Acknowledgments

This material is based upon work supported by the U S Department of Energy, Office of Science, Office of Basic Energy Sciences under contract number DE-AC05-00OR22725 by the Laboratory Directed Research and Development Program of Oak Ridge National Laboratory, managed by UT-Battelle, LLC, for the US Department of Energy (AVI, OSO). ToF SIMS, and AFM measurements were performed at the Center for Nanophase Materials Sciences, which is a DOE Office of Science User Facility. JCA acknowledges support from the Army Research Office under grant W911NF-14-1-0104. GAV acknowledges support from the National Science Foundation under grant DMR-1708615. LWM acknowledges support from the National Science Foundation under grant DMR-1608938.

Notice

This manuscript has been authored by UT-Battelle, LLC, under Contract No. DE-AC0500OR22725 with the U.S. Department of Energy. The United States Government retains and the publisher, by accepting the article for publication, acknowledges that the United States Government retains a non-exclusive, paid-up, irrevocable, world-wide license to publish or reproduce the published form of this manuscript, or allow others to do so, for the United States Government purposes only. The Department of Energy will provide public access to these results of federally sponsored research in accordance with the DOE Public Access Plan (<http://energy.gov/downloads/doe-public-access-plan>).

ORCID iDs

Anton V Ievlev  <https://orcid.org/0000-0003-3645-0508>
Sergei V Kalinin  <https://orcid.org/0000-0001-5354-6152>

References

- [1] Baibich M N, Broto J M, Fert A, Vandau F N, Petroff F, Eitenne P, Creuzet G, Friederich A and Chazelas J 1988 Giant magnetoresistance of (001)Fe/(001)Cr magnetic superlattices *Phys. Rev. Lett.* **61** 2472–5
- [2] Jin S, Tiefel T H, McCormack M, Fastnacht R A, Ramesh R and Chen L H 1994 Thousandfold change in resistivity in magnetoresistive La–Ca–Mn–O films *Science* **264** 413–5
- [3] Kang M, Kim Y-A, Yun J-M, Khim D, Kim J, Noh Y-Y, Baeg K-J and Kim D-Y 2014 Stable charge storing in two-dimensional MoS₂ nanoflake floating gates for multilevel organic flash memory *Nanoscale* **6** 12315–23
- [4] Moodera J S, Kinder L R, Wong T M and Meservey R 1995 Large magnetoresistance at room-temperature in ferromagnetic thin-film tunnel-junctions *Phys. Rev. Lett.* **74** 3273–6
- [5] Gregg J F, Allen W, Ounadjela K, Viret M, Hehn M, Thompson S M and Coey J M D 1996 Giant magnetoresistive effects in a single element magnetic thin film *Phys. Rev. Lett.* **77** 1580–3
- [6] Garcia V et al 2010 Ferroelectric control of spin polarization *Science* **327** 1106–10
- [7] Maksymovych P, Jesse S, Yu P, Ramesh R, Baddorf A P and Kalinin S V 2009 Polarization control of electron tunneling into ferroelectric surfaces *Science* **324** 1421–5
- [8] Gruverman A et al 2009 Tunneling electroresistance effect in ferroelectric tunnel junctions at the nanoscale *Nano Lett.* **9** 3539–43
- [9] Zhuravlev M Y, Sabirianov R F, Jaswal S S and Tsymbal E Y 2005 Giant electroresistance in ferroelectric tunnel junctions *Phys. Rev. Lett.* **94** 4
- [10] Makhlin Y, Schon G and Shnirman A 2001 Quantum-state engineering with Josephson-junction devices *Rev. Mod. Phys.* **73** 357–400
- [11] Greiner M, Mandel O, Esslinger T, Hansch T W and Bloch I 2002 Quantum phase transition from a superfluid to a Mott insulator in a gas of ultracold atoms *Nature* **415** 39–44
- [12] Yoffe A D 2001 Semiconductor quantum dots and related systems: electronic, optical, luminescence and related properties of low dimensional systems *Adv. Phys.* **50** 1–208
- [13] Lin H, Wray L A, Xia Y Q, Xu S Y, Jia S A, Cava R J, Bansil A and Hasan M Z 2010 Half-Heusler ternary compounds as new multifunctional experimental platforms for topological quantum phenomena *Nat. Mater.* **9** 546–9
- [14] Zhang Y et al 2010 Crossover of the three-dimensional topological insulator Bi₂Se₃ to the two-dimensional limit *Nat. Phys.* **6** 584–8
- [15] Chrisey D B and Hubler G K 1994 *Pulsed Laser Deposition of Thin Films* (New York: Wiley)
- [16] George S M 2010 Atomic layer deposition: an overview *Chem. Rev.* **110** 111–31
- [17] Brune H 2013 Epitaxial growth of thin films *Surface and Interface Science* ed K Wandelt vol 4 (Weinheim, Germany: Wiley)
- [18] McDonnell L A and Heeren R M A 2007 Imaging mass spectrometry *Mass Spectrom. Rev.* **26** 606–43
- [19] Chabala J M, Soni K K, Li J, Gavrilov K L and Levi-Setti R 1995 High-resolution chemical imaging with scanning ion probe SIMS *Int. J. Mass Spectrom.* **143** 191–212
- [20] Pacholski M L and Winograd N 1999 Imaging with mass spectrometry *Chem. Rev.* **99** 2977–3006
- [21] Ievlev A V, Maksymovych P, Trassin M, Seidel J, Ramesh R, Kalinin S V and Ovchinnikova O S 2016 Chemical state evolution in ferroelectric films during tip-induced polarization and electroresistive switching *ACS Appl. Mater. Interfaces* **8** 29588–93
- [22] Ganpule C S, Stanishkevsky A, Su Q, Aggarwal S, Melngailis J, Williams E and Ramesh R 1999 Scaling of ferroelectric properties in thin films *Appl. Phys. Lett.* **75** 409–11

- [23] Chang L W, Alexe M, Scott J F and Gregg J M 2009 Settling the 'dead layer' debate in nanoscale capacitors *Adv. Mater.* **21** 4911
- [24] Chang L W, McMillen M, Morrison F D, Scott J F and Gregg J M 2008 Size effects on thin film ferroelectrics: experiments on isolated single crystal sheets *Appl. Phys. Lett.* **93** 132904
- [25] Ievlev A V, Jesse S, Morozovska A N, Strelcov E, Eliseev E A, Pershin Y V, Kumar A, Shur V Y and Kalinin S V 2014 Intermittency, quasiperiodicity and chaos in probe-induced ferroelectric domain switching *Nat. Phys.* **10** 59–66
- [26] Ievlev A V, Morozovska A N, Shur V Y and Kalinin S V 2014 Humidity effects on tip-induced polarization switching in lithium niobate *Appl. Phys. Lett.* **104** 092908
- [27] Ievlev A V, Morozovska A N, Eliseev E A, Shur V Y and Kalinin S V 2014 Ionic field effect and memristive phenomena in single-point ferroelectric domain switching *Nat. Commun.* **5** 5545
- [28] Dahan D, Molotskii M, Rosenman G and Rosenwaks Y 2006 Ferroelectric domain inversion: the role of humidity *Appl. Phys. Lett.* **89** 152902
- [29] Wang R V et al 2009 Reversible chemical switching of a ferroelectric film *Phys. Rev. Lett.* **102** 047601
- [30] Jesse S, Baddorf A P and Kalinin S V 2006 Switching spectroscopy piezoresponse force microscopy of ferroelectric materials *Appl. Phys. Lett.* **88** 062908
- [31] Ievlev A V, Nikolaeva E V, Shishkin E I and Shur V Y 2010 Shape of local hysteresis loops measured by means of piezoresponse force microscopy *Ferroelectrics* **398** 26–33
- [32] Gruverman A and Kholkin A 2006 Nanoscale ferroelectrics: processing, characterization and future trends *Rep. Prog. Phys.* **69** 2443
- [33] Kalinin S V, Morozovska A N, Chen L Q and Rodriguez B J 2010 Local polarization dynamics in ferroelectric materials *Rep. Prog. Phys.* **73** 056502
- [34] Soergel E 2011 Piezoresponse force microscopy (PFM) *J. Phys. D: Appl. Phys.* **44** 464003
- [35] Gruverman A, Auciello O and Tokumoto H 1996 Scanning force microscopy for the study of domain structure in ferroelectric thin films *J. Vac. Sci. Technol. B* **14** 602–5